The Dynamics of Helicopters with Nonlinearities on the Fuselage

Cesar A. B. da SILVA[1]

[1]School of Mechanical Engineering, UFU - Federal University of Uberlândia, Brazil
cabdasr@hotmail.com

Leonardo SANCHES[2*], Guilhem MICHON [2+]

[2]Université de Toulouse, ICA, CNRS, ISAE-Supaero, Toulouse, France
[*] leonardo.sanches@isae-supaero.fr, [+] guilhem.michon@isae-supaero.fr

Abstract

The present paper aims at evaluating the influence of nonlinearities on the dynamic response of an helicopter on the ground. Indeed, the helicopter on the ground might be faced to resonance and instability conditions that could lead to high vibration levels. Nonetheless, under the effects of nonlinearities, the dynamical behaviour of the aircraft could have substantial changes in which quasi-periodic and/or chaotic motions can occur. Poincaré section and bifurcation diagrams are evaluated for different helicopter configurations in order to highlight the dynamical behavior of helicopters with nonlinearities in the fuselage.

1 Introduction

Concerning the helicopter dynamics, one aims avoiding any rise of vibration level during operational conditions. For this purpose, the comprehension of the dynamics of the mechanical components and how they interact with the environment are necessaries. Beyond these aspects, the interaction of the helicopter with the terrain during take-off and landing can cause multiples resonances which might lead to ground resonance with fatal consequences [13, 2].

In order to suppress the ground resonance, among other existent means, elastomeric dampers can play a significant role in the stability of the aircraft. Therefore, the modeling of the elastomeric lag dampers have received increasing attention, specially concerning its nonlinear characteristics [1, 6, 4]. For example, Gandhi and Chopra [1] place an additional nonlinear spring in series with the linear, parallel spring and dashpot in order to represent the elastomeric dampers. Other possibility is to consider the inclusion of pneumatic elements on the aircraft suspension for absorbing and dissipating the vibrating energy [13].

Nonetheless, these dissipative elements and some structural ones introduce nonlinearities that might substantially affect the dynamics of the helicopter [5].

It is known from the literature that rotating machines under nonlinear operating characteristics could attain other than the periodic motion, predictable for linear systems, such as the quasi-periodic or chaotic motions. Recently, Varney and Green observed the presence of quasi-periodic and chaos on the rotor dynamics by assuming rotor-stator contact [14]. Indeed this phenomenon is observed since precisely manufactured bearings are used and thus reduced clearances are imposed for improving the performance of the rotating machines.

Under the hypothesis of nonlinearities for the ground resonance modelling purposes, this paper aims verifying, their effects on the helicopter response. if at certain operating conditions or design properties, the appearance of non-periodic and/or chaotic motion are reached. The helicopter considered contains nonlinear spring stiffness on the fuselage displacements (longitudinal and lateral). The four-bladed rotor consider rigid structures having only lead-lag oscillations. Parametric analyses combined with examination of the Poincaré maps and bifurcation diagrams, the nonlinear dynamical behavior of the helicopter was assessed.

2 Mechanical Modeling

The physical model of the helicopter is based on that presented by [10]. The hypotheses assumed are sufficient for computing accurately (through a linear model) the ground resonance instability of an helicopter with four ($N_b = 4$) articulated bladed rotor.

The aircraft is considered having two translation movements, along x and y-directions (i.e.: $x(t)$ and $y(t)$, respectively) for the fuselage and the angular displacement of each blade ($\varphi_k(t)$,k=1..4). Moreover, it is supposed that the fuselage and blades structures are sufficiently rigid in which they can be modeled as rigid body. No aerodynamic effects are take into account and the rotor speed is assumed constant Ω.

The blades are connected to rotor hub through a hinge axis. At each blade hinge, a set of spring (K_{bk}) and damper (C_{bk}) elements is placed. The landing skids are represented by a set of nonlinear elastic and linear viscous damping forces in both directions of the fuselage movements. Indeed, the nonlinear elastic function can represent the different sources of nonlinearities, e.g.: suspensions forces, lading skid structure or the soil restitution force. In the nonlinear elastic force acting on the fuselage, the k_{fx} and k_{fy} are the coefficients of the linear terms, while k_{nlx} and k_{nly} are the coefficients of the cubic ones. Others polynomial orders are not considered in the present work. The damping coefficients are c_{fx} and c_{fy} along the x and y directions, respectively. The Figure 1 sketches the mechanical model adopted for the helicopter.

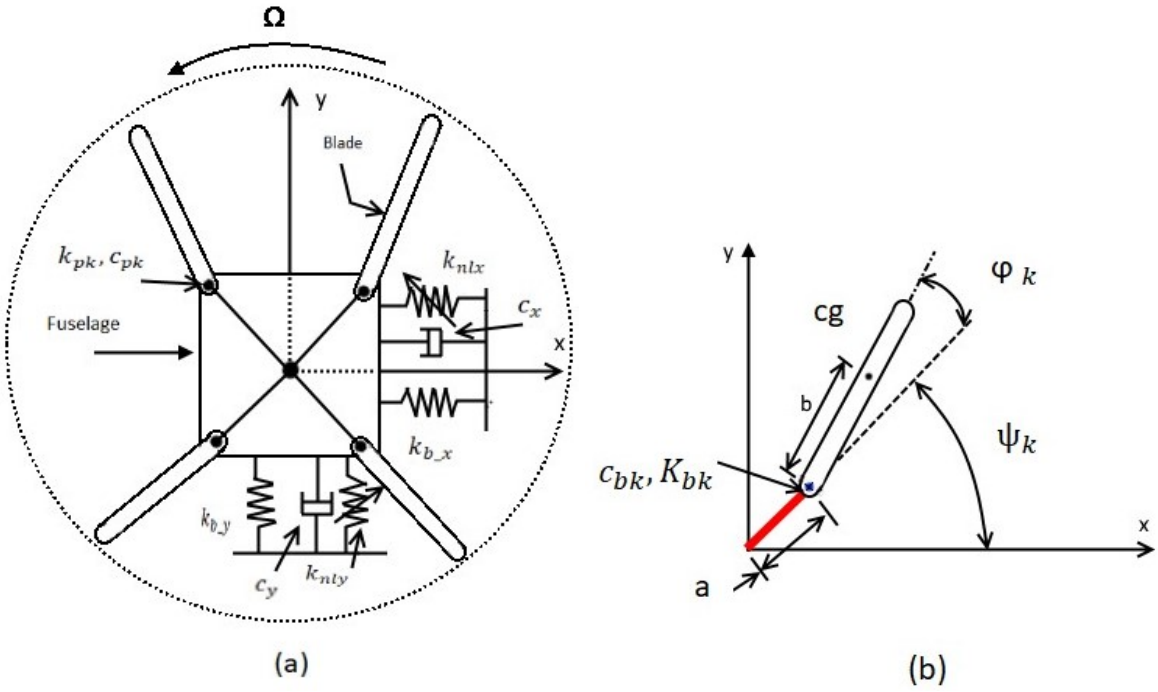

Figure 1 – Sketch of Helicopter Mechanical Model

The equations of motion are obtained through the Lagrange equation [10, 9, 15] applied at the kinetic and potential energies expressions and by considering the virtual work of the non-conservative forces on the system. Under the hypothesis of small angular displacements $\varphi_k(t)$, the trigonometric terms can be reduced to linear expressions when small perturbation theory is considered [9]. Thus, the linear matrix equation, Eq. 1, can be easily determined as:

$$\mathbf{M}(t)\ddot{\mathbf{u}} + \mathbf{G}(t)\ddot{\mathbf{u}} + \mathbf{K}(t)\mathbf{u} = \mathbf{F_{nl}} \tag{1}$$

with $\mathbf{M}(t)$, $\mathbf{G}(t)$ and $\mathbf{K}(t)$ are the mass, damping / gyroscopic and stiffness matrix. The vector $\mathbf{u}$ corresponds to $[x(t), y(t), \varphi_1(t), \varphi_2(t), \varphi_3(t), \varphi_4(t)]^T$ which are the helicopter degrees of freedom. The $\mathbf{F_{nl}}$ represents the vector of nonlinear terms of the helicopter model.

It is important to note the time dependence of the matrices since the blades angular displacements are given on a rotating frame while fuselage movements are described in the inertial one. Using the Multi-blade coordinate transformation as showed in [12, 11], such time dependent matrix might be reduced to one with constant coefficients. The new vector of generalized coordinates $\mathbf{q}(t)$ is obtained through the following relation:

$$\mathbf{q}(t) = \mathbf{T(t)}\ \mathbf{u}(t) \tag{2}$$

with,

$$[\mathbf{T(t)}] = \begin{bmatrix} 1 & 0 & 0 & 0 & 0 & 0 \\ 0 & 1 & 0 & 0 & 0 & 0 \\ 0 & 0 & 1 & 1 & \cos(\Omega t) & \sin(\Omega t) \\ 0 & 0 & 1 & -1 & -\sin(\Omega t) & \cos(\Omega t) \\ 0 & 0 & 1 & 1 & -\cos(\Omega t) & -\sin(\Omega t) \\ 0 & 0 & 1 & -1 & \sin(\Omega t) & -\cos(\Omega t) \end{bmatrix} \tag{3}$$

Once the Eq.3 has been replaced in Eq.1, after some mathematical manipulations, the helicopter dynamics is given by:

$$\mathbf{M_C}\ddot{\mathbf{q}} + \mathbf{G_C}\dot{\mathbf{q}} + \mathbf{K_C}\mathbf{q} = \mathbf{F_{nl}} \tag{4}$$

where,

$$\mathbf{M_C} = \begin{bmatrix} m_f + N_b m_b & 0 & 0 & 0 & -2\,b\,m_b & 0 \\ 0 & m_f + N_b m_b & 0 & 0 & 0 & 2\,b\,m_b \\ 0 & 0 & N_b\,(m_b b^2 + I_{zb}) & 0 & 0 & 0 \\ 0 & 0 & 0 & N_b\,(m_b b^2 + I_{zb}) & 0 & 0 \\ -2\,b\,m_b & 0 & 0 & 0 & N_b/2(m_b b^2 + I_{zb}) & 0 \\ 0 & 2\,b\,m_b & 0 & 0 & 0 & N_b/2(m_b b^2 + I_{zb}) \end{bmatrix} \tag{5}$$

$$\mathbf{G_C} = \begin{bmatrix} c_x & 0 & 0 & 0 & 0 & 0 \\ 0 & c_y & 0 & 0 & 0 & 0 \\ 0 & 0 & N_b c_b & 0 & 0 & 0 \\ 0 & 0 & 0 & N_b c_b & 0 & 0 \\ 0 & 0 & 0 & 0 & N_b/2\,c_b & -N_b\,(m_b b^2 + I_{zb})\,\Omega \\ 0 & 0 & 0 & 0 & N_b\,(m_b b^2 + I_{zb})\,\Omega & N_b/2\,c_b \end{bmatrix} \tag{6}$$

$$\mathbf{K_C} = \begin{bmatrix} k_{fx} & 0 & 0 & 0 & 0 & 0 \\ 0 & k_{fy} & 0 & 0 & 0 & 0 \\ 0 & 0 & N_b\,(k_b + \Omega^2 a b m_b) & 0 & 0 & 0 \\ 0 & 0 & 0 & N_b\,(k_b + \Omega^2 a b m_b) & 0 & 0 \\ 0 & 0 & 0 & 0 & k_\tau & -\,c_b\,\Omega N_b/2 \\ 0 & 0 & 0 & 0 & c_b\,\Omega N_b/2 & k_\tau \end{bmatrix} \tag{7}$$

with $k_\tau = N_b/2(k_b + \Omega^2(a\,b\,m_b - I_{zb} - b^2 m_b))$ and $\mathbf{q} = [x(t), y(t), \tau_d(t), \tau_0(t), \tau_{1c}(t), \tau_{1s}(t)]^T$. The variables $\tau_d(t)$, $\tau_0(t)$, $\tau_{1c}(t)$, and $\tau_{1s}(t)$ are related to rotor modes of vibration and they replace the blade displacements on generalized coordinate vector. Through this coordinate transformation, the Eq. 1 becomes time-invariant (*c.f.* Eq.4).

3 Linear Stability Analysis

Several authors have addressed to the stability analysis of the ground resonance previously by considering linear dynamical models [15, 4]. Indeed, the stability analysis of the ground resonance will contribute for further comprehension of the behavior of the nonlinear dynamical system. Therefore, present section aims at verifying the stability of the linear LTI system by neglecting the nonlinear efforts $\mathbf{F}_{nl}$ from Eq. 4. The mechanical data for the stability analysis are given in Tab. 1.

It is important to note that the natural frequencies and damping factors written in Tab. 1 are defined with respect to the helicopter dynamical properties at rest with null rotor speed. Thus,

$$\omega_x = \sqrt{k_{fx}/(m_f + N_b m_b)} \qquad \omega_y = \sqrt{k_{fy}/(m_f + N_b m_b)} \qquad \omega_b = \sqrt{k_b/(I_{zb} + b^2 m_b)} \tag{8}$$

$$c_x = 2\xi_x \omega_x (m_f + N_b m_b) \qquad c_y = 2\xi_y \omega_y (m_f + N_b m_b) \qquad c_b = 2\xi_b \omega_b (I_{zb} + b^2 m_b) \tag{9}$$

Property	Value	Units
m_f	2902	kg
m_b	31.9	kg
Iz_b	259	kg m^2
a	0.2	m
b	2.5	m
ω_x	6π	rad/s
ω_{bk} ($k = 1 \ldots 4$)	3π	rad/s
$\xi_x = \xi_y = \xi_{bk}$	0.1	%

Table 1 – Helicopter's Data

The stability boundaries are verified through the eigenvalues (ρ) of the linear system investigated for several rotor speed values (i.e., $0 \leq \Omega \leq 10$ Hz) and for three fuselage configurations, i.e: $\omega_y = [6, 7, 8]$ Hz. The results are illustrated in Figs. 2a to 2c for $\omega_y = 6$, 7 and 8 Hz, respectively.

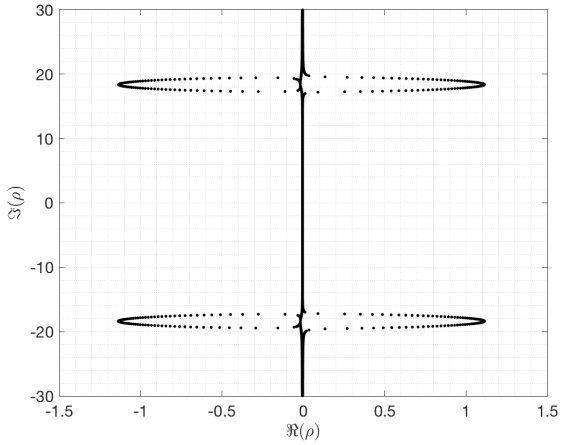

(a) $\omega_y = 6\pi$

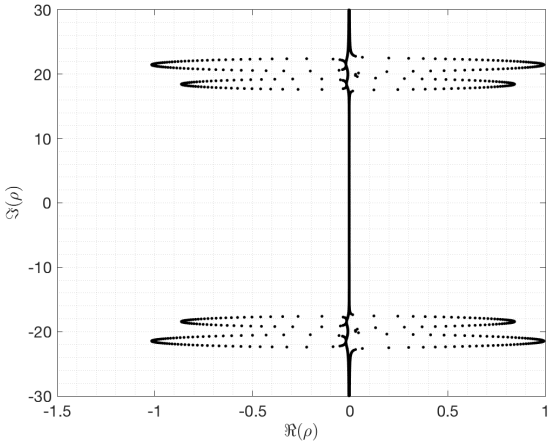

(b) $\omega_y = 7\pi$

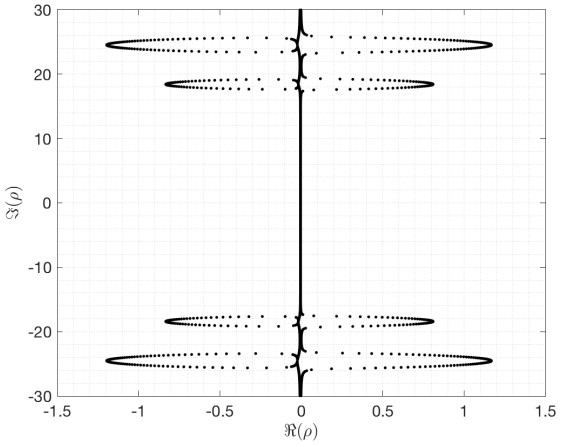

(c) $\omega_y = 8\pi$

Figure 2 – Eigenvalue Evolution with respect to rotor speed and fuselage configurations.

One notice from each graph the changes of the natural frequencies and exponential decay constant of the dynamical system once the parameter (rotor speed) varies. For the three fuselage configurations analyzed, clearly it can be pointed out the existence of unstable regions (i.e., $\mathscr{R}(\rho) > 0$) for certain range of rotor speed values. These unstable regions are associated with the natural frequencies of the fuselage at rest. As the natural frequencies of the fuselage along x and y directions become dissimilar (*c.f.* Fig. 2b-2c), the instability

regions evolve leading to clearly two distinct zones: each one is related to each direction of fuselage oscillation. Nonetheless, when the fuselage frequencies are equals (i.e., $\omega_x = \omega_y$), the instability regions are then superposed. Specially concerning this last case, it is observed that two pairs of eigenvalues become unstable simultaneously, indicating the existence of double hopf bifurcation. Otherwise, only one pair of eigenvalue becomes unstable and therefore a single hopf bifurcation happens.

In order to determine the critical rotating speeds for each fuselage configuration, Figure 3 shows the maximum real part of the eigenvalues with respect to the rotor speed. The boundaries of instabilities are determined by inspecting when positive values are attained for the real part of the eigenvalues. The instability region for

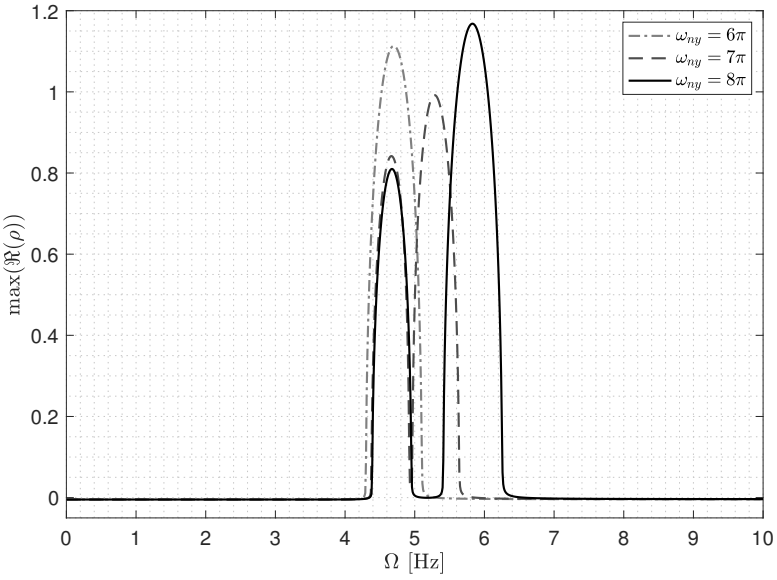

Figure 3 – Instability boundaries for different fuselage configurations

$\omega_y = 6\pi$ are given for rotor speed values within $4.25 < \Omega < 5.3$ Hz. When the fuselage natural frequency is changed to $\omega_y = 7\pi$, the critical speeds are within $4.33 < \Omega < 5.87$ Hz. Finally, when $\omega_y = 8\pi$, there are two unstable regions identified, i.e., $4.35 < \Omega < 5.08$ Hz and $5.23 < \Omega < 6.56$ Hz.

4 Bifurcation Diagrams

The present section aims at analyzing the effects of the nonlinear efforts on the dynamic response of the helicopter. Indeed, the restoring forces from the pneumatic components presented in some helicopter suspensions can be expressed through nonlinear functions [13, 7, 6]. In addition, for some cases, the interactions between the soil and aircraft might cause nonlinear efforts [2]. For this purpose, one assumes a pure cubic polynomial function acting along the fuselage displacements with the following coefficients $k_{nlx} = k_{nly} = 1x10^5 N/m^3$.

Since hopf bifurcation points on the helicopter dynamics were evidenced from the linear stability analysis (*c.f.* section 3), the literature shows that hopf bifurcation might leads to periodic motion which characterizes the limit cycle oscillations. Nonetheless, the periodic motion can evolve under control parameter variation and becomes into non-periodic one. It can further evolve from the non-periodic motion to a chaotic motion [3]. Therefore, Poincaré sections and bifurcation diagrams are evaluated from the time history data obtained through the numerical integration of the nonlinear equations (*c.f.,* Equation 4). The initial condition is the same for all simulations and it considers a shift of $0.1m$ for the fuselage displacements from the equilibrium position, while others displacements and speeds are nulls. The Poincaré section is considered into the plane $\tau_c = 0$. Henon algorithm is used for precisely obtain the points intercepting the Poincaré section and, therefore, used to obtain the bifurcation diagrams [8].

Figures 4 and 5 describe the bifurcation diagram for $x(t)$ and $y(t)$ with respect to Ω for the helicopter with identical natural frequencies of the fuselage (i.e., ω_x and ω_y are 6π rad/s). Since the Poincaré sections are evaluated in the plane $\tau_c = 0$, and thus for the bifurcation diagrams, one observes that $y(t)$ reaches higher amplitude level than $x(t)$, accordingly to Figures 4a) and 4b). This fact might be explained since the variables

$x(t)$ and $\tau_c(t)$ are in-phase motion, while $y(t)$ is quarter phase with $\tau_c(t)$. Moreover, concerning Figure 5 at $\Omega = 4.865$ Hz, the values of $x(t)$ and $y(t)$ are concentrated at some points instead of being uniformly distributed, as it can be evidenced for the whole rotor speed conditions analyzed. A closer investigation is carried out for comprehending the differences between the two cited cases. Therefore, the Poincaré section and the phase subspace for $\Omega = 4.85$ Hz and $\Omega = 4.865$ Hz are represented in Figures 6 and 7. Clearly, by comparing the Poincaré sections for two speed conditions, the Figure 6a represents a quasi-periodic behavior while at Figure 7a a periodic signal with nine harmonics is observed.

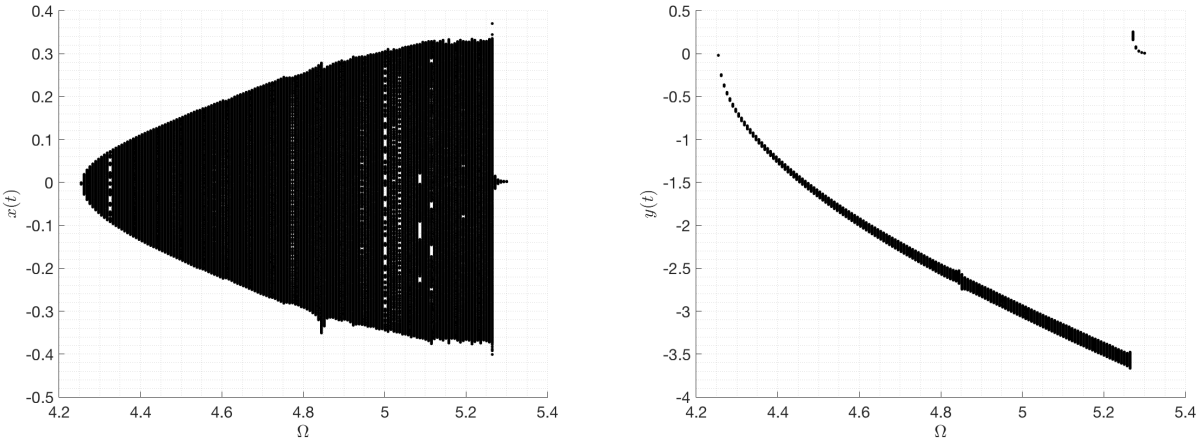

(a) (b)

Figure 4 – Bifurcation Diagram for $\omega_x = 6\pi$ and $\omega_y = 6\pi$: a) $x(t)$ and b) $y(t)$

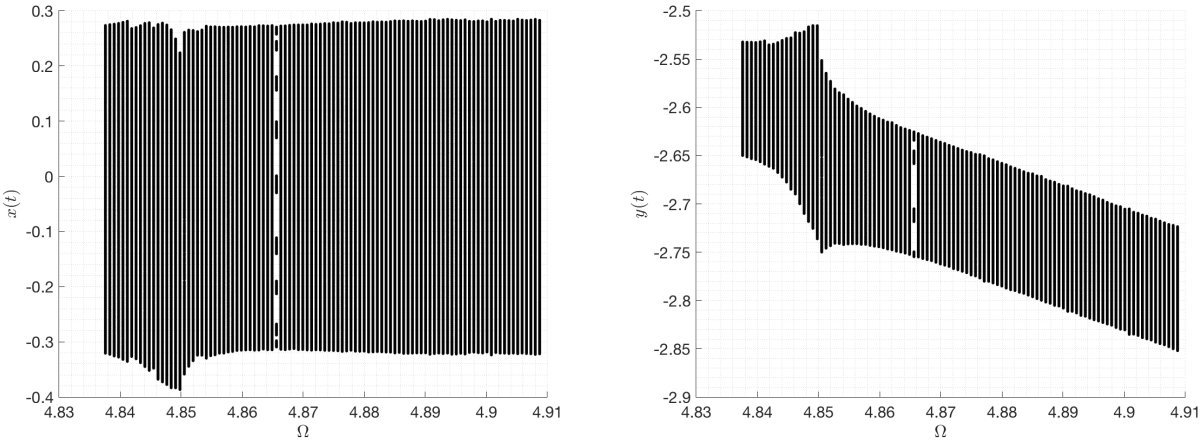

(a) (b)

Figure 5 – Detailed Bifurcation Diagram for $\omega_x = 6\pi$ and $\omega_y = 6\pi$: a) $x(t)$ and b) $y(t)$

The helicopter is now considered to have an asymmetry between the frequencies of the fuselage i.e., the oscillations along x-direction is at $\omega_x = 6\pi$ rad/s while in y-direction it is at $\omega_y = 7\pi$ rad/s. The influence of the nonlinearity in the fuselage on the helicopter is evidenced through the bifurcation diagram in Figure 8. One observes that, as Ω increases, the bifurcation amplitude levels for x and y are also augmenting. At $\Omega = 5.4$ there is no movements noted, since the helicopter are nearly stable (*c.f.* Figure 3). Moreover, the amplitudes of the bifurcation section get increased for rotor speeds higher than 5.66 Hz. Figure 9 compares the evolution of the Poincaré sections for different rotor speed values in order to highlight the increment of the amplitude level on the bifurcation diagram. A closer inspection on the time response is done through Figure 10 in which a slight modulation of the signal for $\Omega = 5.59$ Hz is observed; while for $\Omega = 5.82$ Hz the signal modulation has significantly changed.

Finally, the helicopter with high asymmetry level on the fuselage frequencies is investigated, i.e., $\omega_x = 6\pi$

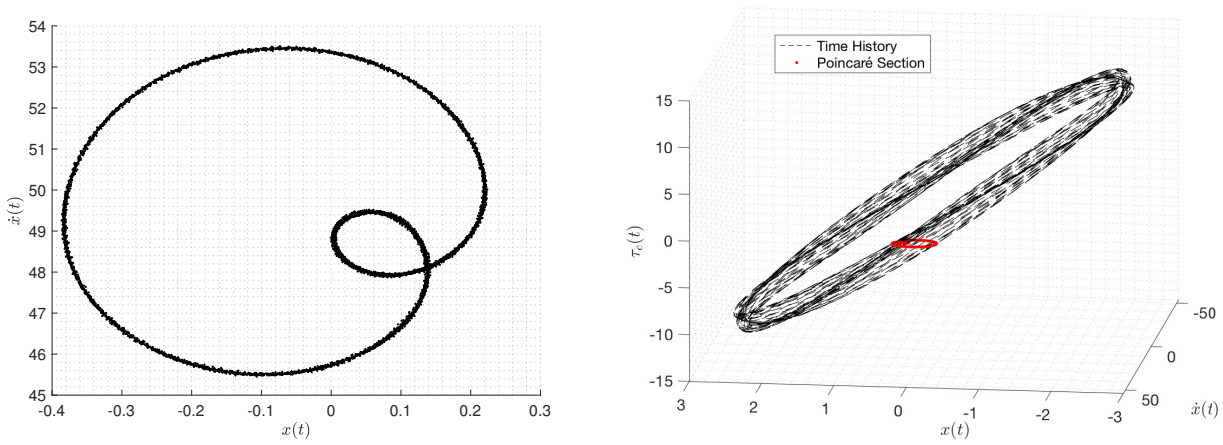

(a) Poincaré Section

(b) Phase Subspace

Figure 6 – Poincaré section and phase subspace at $\Omega = 4.85$ Hz of an helicopter with $\omega_x = 6\pi$ and $\omega_y = 6\pi$

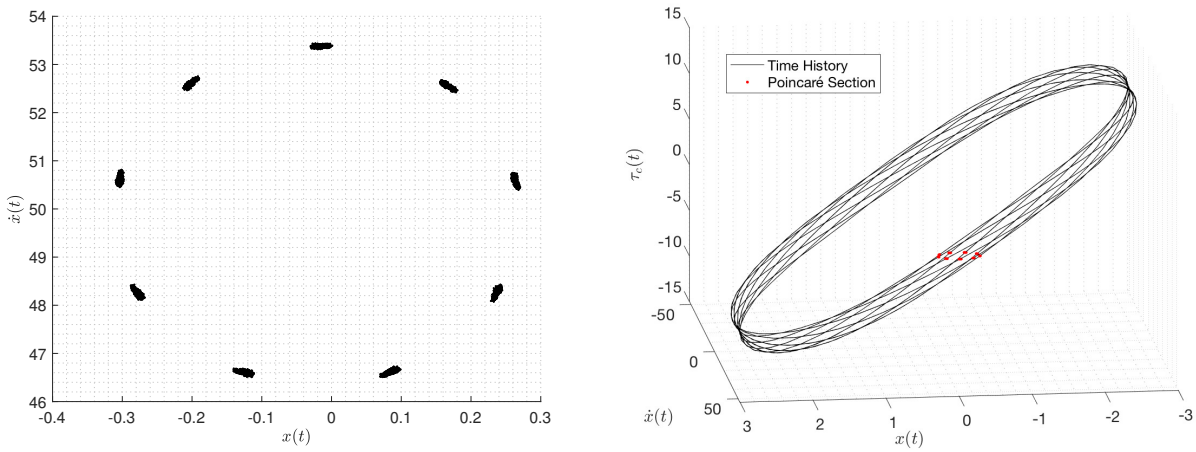

(a) Poincaré Section

(b) 3D- Phase Subspace

Figure 7 – Poincaré section and phase subspace at $\Omega = 4.865$ Hz of an helicopter with $\omega_x = 6\pi$ and $\omega_y = 6\pi$

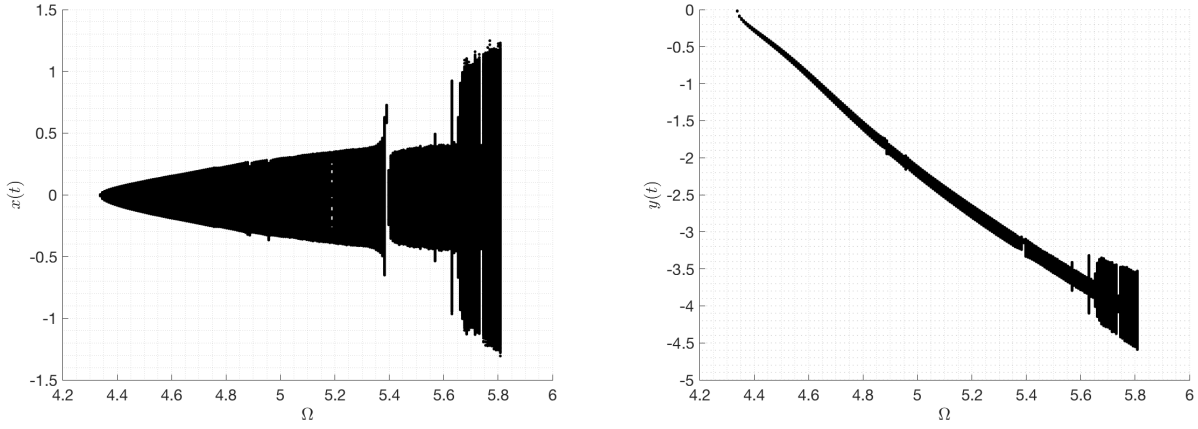

(a) (b)

Figure 8 – Bifurcation Diagram for $\omega_x = 6\pi$ and $\omega_y = 7\pi$: a) $x(t)$ and b) $y(t)$

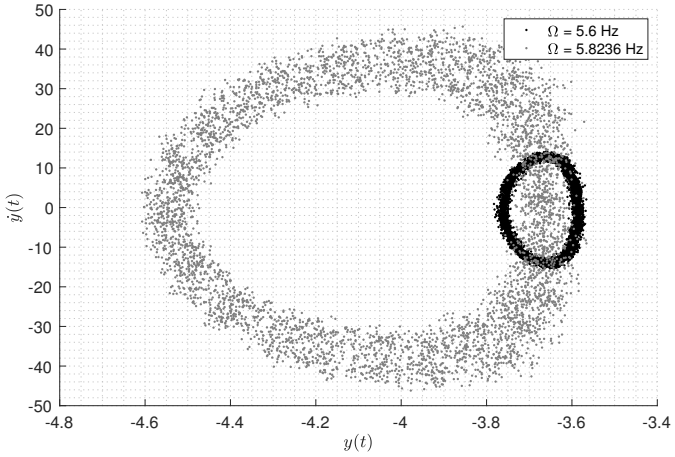

Figure 9 – Comparison of Poincaré Sections for Helicopter with $\omega_x = 6\pi$ and $\omega_y = 7\pi$

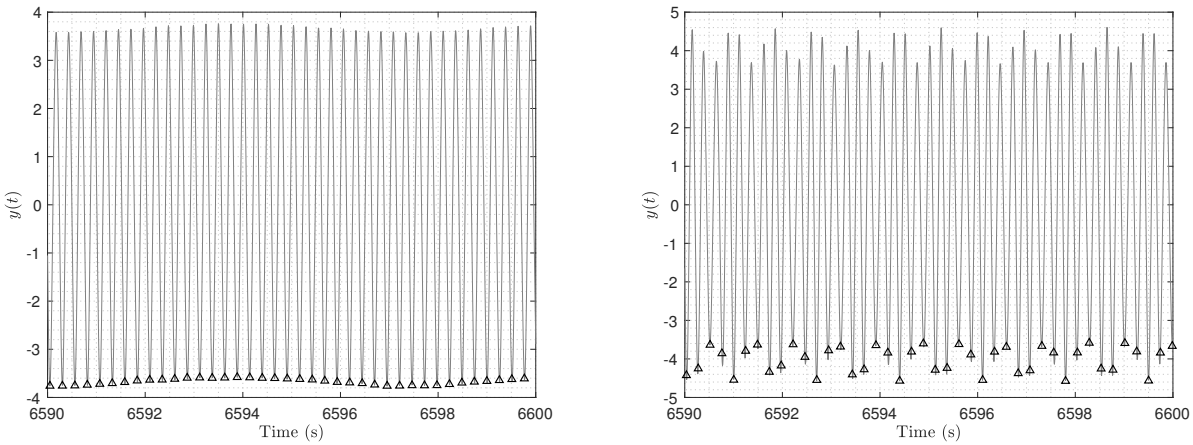

(a) $\Omega = 5.59$ Hz (b) $\Omega = 5.82$ Hz

Figure 10 – Temporal Responses of the helicopter with $\omega_x = 6\pi$ and $\omega_y = 7\pi$ - Δ Poincaré section points

rad/s and $\omega_y = 8\pi$ rad/s. The bifurcation diagram for such dynamical system under the nonlinear efforts are presented in Figure 11. The reader should note that for $5.08 \leq \Omega \leq 5.23$ Hz there is no amplitudes on the bifurcation diagram since the helicopter is stable and thus the response converges to zero (static equilib-

rium). Moreover, similar to the previous helicopter configuration analyzed (i.e., helicopter with $\omega_x = 6\pi$ rad/s and $omega_y = 7\pi$ rad/s), there exist some regions in the bifurcation diagram in which the amplitudes growth abruptly. A closer inspection of some of these regions is carried out. For this purpose, the Poincaré sections were investigated for $\Omega = 5.9,\ 6.0,\ 6.34$ and 6.48 Hz. Beyond the amplitude level that changed as function of the rotor speed, one observe that for $\Omega = 6.34$ Hz the points on the Poincaré section are distributed along likely two circumferences.

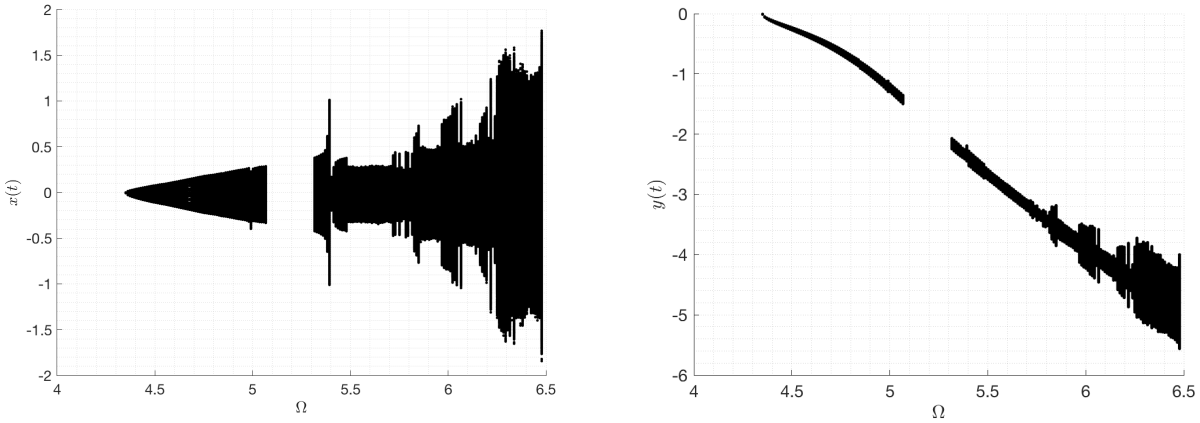

(a) (b)

Figure 11 – Bifurcation Diagram for $\omega_x = 6\pi$ and $\omega_y = 8\pi$: a) $x(t)$ and b) $y(t)$

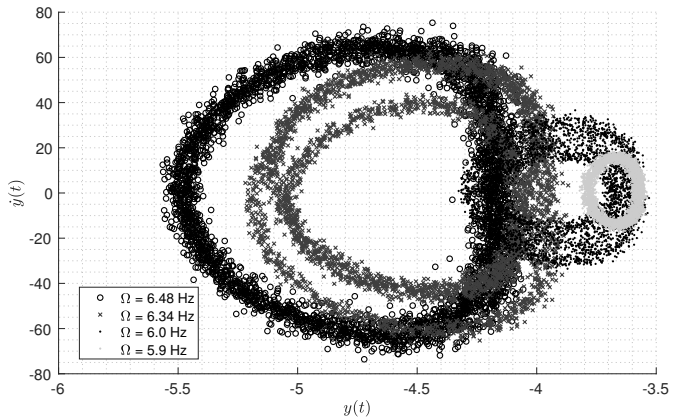

Figure 12 – Comparison of Poincaré Sections of a Helicopter with $\omega_x = 6\pi$ and $\omega_y = 8\pi$

5 Conclusions

The present paper aims at analyzing the effects of the nonlinear efforts on the dynamic response of the helicopter on the ground. The nonlinearities might change the behavior of the dynamical system, in which other than periodic motion is attained. Through the analysis, this paper investigated if non-periodic or chaotic motions are observed for the helicopter.

For this purpose, Poincaré sections and bifurcations diagrams were done for different helicopter configurations. Three different sets of fuselage's natural frequencies were evaluated, accordingly to the value of ω_y adopted.

The bifurcation diagrams highlight that for some rotor speed values, an abruptly rise in amplitude was observed for asymmetric fuselage configuration. For some exception cases where periodic motion was attained, non-periodic motion occurs for several rotor speeds values.

References

[1] GANDHI, F., AND CHOPRA, I. Elastomeric lag damper effects on flap-lag stability in forward flight. In *35th Structures, Structural Dynamics, and Materials Conference* (1994), p. 1311.

[2] GUALDI, S., MASARATI, P., MORANDINI, M., AND GHIRINGHELLI, G. L. A multibody approach to the analysis of helicopter-terrain interaction. In *Proceedings of 28th European Rotorcraft Forum, Bristol, UK* (2002).

[3] HILBORN, R. C., ET AL. *Chaos and nonlinear dynamics: an introduction for scientists and engineers*. Oxford University Press on Demand, 2000.

[4] KIM, S. J., AND YUN, C. Y. Performance comparison between piezoelectric and elastomeric lag dampers on ground resonance stability of helicopter. *Journal of Intelligent Material Systems and Structures 12*, 4 (2001), 215–222.

[5] KING, R. L. Nonlinear inplane flexbeam stiffness provides rotor system stability without lag dampers. *Journal of the American Helicopter Society 46*, 4 (2001), 283–289.

[6] KUNZ, L. Influence of elastomeric damper modeling on the dynamic response of helicopter rotors. *AIAA journal 35*, 2 (1997), 349–354.

[7] LIU, Y., WANG, J., AND TONG, Y. Kinetic analysis of elastomeric lag damper for helicopter rotors. *IOP Conference Series: Materials Science and Engineering 311*, 1 (2018), 012006.

[8] PALANIYANDI, P. On computing poincaré map by hénon method. *Chaos, Solitons & Fractals 39*, 4 (2009), 1877–1882.

[9] SANCHES, L., MICHON, G., BERLIOZ, A., AND ALAZARD, D. Parametrically excited helicopter ground resonance dynamics with high blade asymmetries. *Journal of Sound and Vibration 331*, 16 (2012), 3897–3913.

[10] SANCHES, L., MICHON, G., BERLIOZ, A., AND ALAZARD, D. Helicopter ground resonance phenomenon with blade stiffness dissimilarities: experimental and theoretical developments. *Journal of Vibration and Acoustics 135*, 5 (2013), 051028.

[11] SKJOLDAN, P., AND HANSEN, M. H. On the similarity of the coleman and lyapunov–floquet transformations for modal analysis of bladed rotor structures. *Journal of Sound and Vibration 327*, 3-5 (2009), 424–439.

[12] STOL, K., MOLL, H.-G., BIR, G., AND NAMIK, H. A comparison of multi-blade coordinate transformation and direct periodic techniques for wind turbine control design. In *47th AIAA Aerospace Sciences Meeting including the New Horizons Forum and Aerospace Exposition* (2009), p. 479.

[13] STOLZ, B., BRÖDERMANN, T., CASTIELLO, E., ENGLBERGER, G., ERNE, D., GASSER, J., HAYOZ, E., MÜLLER, S., MUHLEBACH, L., LÖW, T., SCHEUER, D., VANDEVENTER, L., BJELONIC, M., GÜNTHER, F., KOLVENBACH, H., HOPFLINGER, M., AND HUTTER, M. An adaptive landing gear for extending the operational range of helicopters. In *2018 IEEE/RSJ International Conference on Intelligent Robots and Systems (IROS)* (Oct 2018), pp. 1757–1763.

[14] VARNEY, P., AND GREEN, I. Nonlinear phenomena, bifurcations, and routes to chaos in an asymmetrically supported rotorâstator contact system. *Journal of Sound and Vibration 336* (2015), 207 – 226.

[15] WANG, J., AND CHOPRA, I. Dynamics of helicopters in ground resonance with and without blade dissimilarities. In *Dynamics Specialists Conference* (1992), p. 2108.